

GPO PRICE \$ _____

CFSTI PRICE(S) \$ _____

Hard copy (HC) 3.00

Microfiche (MF) .65

653 July 65

Quarterly Progress Report

For Period

September 30 to December 30, 1966

FUNDAMENTAL STUDIES OF THE METALLURGICAL,
ELECTRICAL, AND OPTICAL PROPERTIES OF
GALLIUM PHOSPHIDE

Grant No. NsG-555

Prepared For

NATIONAL AERONAUTICS AND SPACE ADMINISTRATION
LEWIS RESEARCH CENTER
CLEVELAND, OHIO

Work Performed By

Solid-State Electronics Laboratories
Stanford University
Stanford, California

FACILITY FORM 802

N67 18120
(ACCESSION NUMBER)

40
(PAGES)

CP-81790
(NASA CR OR TMX OR AD NUMBER)

(THRU)

(CODE)

(CATEGORY)

PROJECT 5109: SPECTRA OF TRANSITION METALS IN SEMICONDUCTORS

National Aeronautics and Space Administration
Grant NsG 555

Project Leader: G. L. Pearson

Staff: J. Baranowski

Last quarter we reported the spectra of iron in several II-VI compounds and in GaP. We indicated that spectra of iron can be interpreted on the basis of splitting of the energy levels of the d^6 configuration by a weak crystal field. We will report the spectra of divalent iron in CdS and in GaAs, the spectra of nickel in GaP and of cobalt in CdTe, ZnTe, GaAs and GaP taken at liquid helium temperatures. We will also report some general conclusions concerning the interpretation of the d^n configurations in semiconductors.

Optical Spectra of Fe^{+2} in CdS.

Iron was evaporated on both surfaces of the sample and diffused at $1100^\circ C$ for 24 hours. The absorption spectrum of divalent iron in CdS is shown in Fig. 1. To explain the four peaks shown in Fig. 2 it is necessary to take into account the hexagonal structure of CdS. Because of this structure, the sulfide ions do not coordinate the cadmium ions or iron ions (iron substitutes for cadmium [Ref. 1]) in a regular tetrahedron, but experience a slight uniaxial distortion along the optic axis of the crystal. We are assuming that this distortion can be represented as an axial field b in the $\langle 111 \rangle$ direction and is weak compared with the crystal field Dq and the spin-orbit coupling $\lambda L \cdot S$ ($Dq \gg \lambda L \cdot S \gg b$). The splitting of the ground state 5E by spin-orbit coupling of the second order and by the axial field in a $\langle 111 \rangle$ direction is presented in Fig. 3. The splitting

was calculated from matrix elements given by W. Low and M. Weger [Ref. 2]. The fit of the levels from which the transitions are taking place is indicated by arrows. Very good agreement with experiment was obtained for $Dq = 280 \text{ cm}^{-1}$, $\lambda = -95 \text{ cm}^{-1}$ and $b = +70 \text{ cm}^{-1}$.

Optical Spectra of Fe^{+2} in GaAs.

In this study, single crystals of GaAs with an electron concentration of $n = 5 \cdot 10^{17} \text{ cm}^{-3}$ were used. Iron was diffused at 1160°C for 24 hours. The spectrum taken at liquid helium temperature is shown in Fig. 4. The two sharp peaks which appear at the low energy side of the spectrum are connected with transitions from the two lowest levels of the ground state ^5E . By the procedure described in the previous report, we obtain for GaAs:

$$\begin{aligned} Dq &= 319.5 \text{ cm}^{-1}, \\ \text{and } \lambda &= -86 \text{ cm}^{-1}. \end{aligned}$$

The smaller value of Dq compared to GaP is in agreement with that observed in II-VI compounds. Crystals with higher lattice constants have smaller values of Dq .

Conclusions.

Crystal field theory is able to explain very well indeed the splitting of the ground state ^5E of the d^6 configuration in II-VI compounds and III-V compounds. The fine structure which always appears in the low energy side of the spectrum reflects the fine splitting of the ^5E level. The interpretation on the basis of crystal field theory give the exact values of Dq (the crystal field strength parameter) and λ (the spin-orbit coupling constant in the

crystal). The description by crystal field theory of the upper level 5T_2 is not as good as it is in the case of the ground level 5E . The predicted total first order spin-orbit splitting of the 5T_2 level should be $5|\lambda|$. We can expect that width of the absorption band connected with the transition ${}^5E \rightarrow {}^5T_2$ should be of the same order, neglecting the interaction with phonons. The observed width of this absorption band is approximately $10(\lambda)$ (see Table I). In addition, there is some unexplained structure on the absorption band in CdS: Fe and ZnSe: Fe. We found less of this structure in CdTe: Fe and ZnTe: Fe and GaP: Fe and almost none at all in GaAs: Fe.

The two experimental facts mentioned above can be caused by interaction with phonons. They also indicate that the orbitals connected with the 5T_2 state interact more strongly with σ bonding orbitals than the ones connected with the 5E state. Because the point charge model developed by a crystal field theory does not take into account such interactions, we cannot expect an exact agreement with experiment. The transition ${}^5E \rightarrow {}^5T_2$ in a molecular-orbital theory (3) is connected with the transfer of one electron from the e-orbital to the t-orbital: $(t^3e^3 \rightarrow t^4e^2)$. The t-orbitals are directed toward ligands so one can expect a higher degree of interaction with σ bonding orbitals than in the case of e-orbitals which are not directed toward ligands. Thus we can expect 5E states (three electrons on t-orbitals and three on e-orbitals) will be better described by a crystal field theory than the 5T_2 state (four electrons on t and two on e-orbitals). Therefore, we have got much better agreement between theory and experiment for 5E levels than for 5T_2 levels.

Optical Spectra of Ni^{+2} in GaP.

Polycrystalline GaP was used in this study. Nickel was diffused at 1250°C . The spectrum of nickel in GaP taken at liquid helium temperature is shown in Fig. 5. The spectrum can be interpreted as a spectrum of a d^8 configuration in a tetrahedral field. Similar spectra of Ni^{+2} in some II-VI compounds were reported by M. A. Weakliem [Ref. 4]. The free nickel atom has a $4s^2 3d^8$ configuration of electrons and the ground state according to Hund's rule is 3F . The nickel replacing gallium as an impurity contributes two 4s electrons for bonding, leaving a d^8 configuration and an unfilled acceptor level. As in the case of iron in GaP, the third electron needed for bonding is probably taken from a shallow donor if the concentration of such donors is of the same order as the concentration of nickel centers.

The energy level diagram for states of the d^8 configuration split by a crystal field of tetrahedral symmetry and spin-orbit coupling is presented in Fig. 6. The strong absorption close to 1μ we assign to the transition $^3A_1(^3F) \rightarrow ^3T_1(^3P)$. The two peaks at 1.12μ and 1.28μ are connected with transitions $^3A_1 \rightarrow ^3A_2(^3F)$ and $^3A_1 \rightarrow ^1T_2(^1D)$ respectively. We are not able to explain the fine structure which is shown in Fig. 7. Crystal field theory predicts that the $^3T_1(^3P)$ level is split into four levels and the only symmetry allowed transition is to the lowest one, T_2 . The appearance of components with representation other than T_2 violates the selection rule $A_1 \rightarrow T_2$. This may be accomplished by coupling with vibrational modes which cause the forbidden states to be mixed with allowed ones in higher order. Taking into account that the ground state is split

by spin-orbit coupling and assuming that $|\lambda| = 250 \text{ cm}^{-1}$, we obtain the following positions of the energy levels:

$${}^3T_1({}^3F) = 0$$

$${}^3T_1({}^3P) = 9400 \text{ cm}^{-1}$$

$${}^3A_2({}^3F) = 8200 \text{ cm}^{-1}$$

$${}^1T_2({}^1D) = 6900 \text{ cm}^{-1}$$

We can get the best fit to Tanabe and Sugano diagrams assuming $B = 400 \text{ cm}^{-1}$ and $Dq = 420 \text{ cm}^{-1}$. Comparing the values of B and Dq for Ni^{+2} in GaP to Co^{+2} in GaP [Ref. 6] we see that B is higher and Dq is smaller. This is contrary to what was observed in some II-VI compounds [Ref. 4] where the value for Ni^{+2} and Co^{+2} were of the same order and the value of Dq for Ni^{+2} was always higher than for Co^{+2} . To understand this, we measured the spectra of cobalt in GaP, GaAs, CdTe and ZnTe at liquid helium temperatures.

Spectra of Co^{+2} in Semiconductors.

Cobalt was diffused into CdTe and ZnTe for 12 hours at 950°C and into n-type GaAs and GaP for 24 hours at 1100°C and 1300°C . The absorption spectra taken at liquid helium temperatures showed two main absorptions which can be interpreted on the basis of transitions within the d^7 configuration. The energy level diagram for states of the d^7 configuration split by a crystal field of tetrahedral symmetry and spin-orbit coupling is shown in Fig. 8. There are two transitions, ${}^4A_2({}^4F) \rightarrow {}^4T_1({}^4F)$ and ${}^4A_2({}^4F) \rightarrow {}^4T_1({}^4P)$ allowed by spin and symmetry. Both 4T_1 levels are predicted to be split by spin-

orbit coupling into four components. Just beyond the absorption edge there is a strong peak due to the ${}^4A_2({}^4F) \rightarrow {}^4T_1({}^4P)$ transition showing the structure which is more complicated than predicted by spin-orbit splitting. This peak for CdTe: Co is shown in Fig. 9 for ZnTe: Co in Fig. 11, for GaP: Co in Fig. 12 and Fig. 13, and for GaAs: Co in Fig. 14. The spectrum for this transition for GaAs: Co is shown on an expanded scale in Fig. 15 because it is very compressed compared to the others. This indicates that the interaction of electronic orbitals with σ bonding orbitals has a pronounced effect on spin-orbit splitting.

Further into the infrared, there is another absorption due to the ${}^4A_2({}^4F) \rightarrow {}^4T_1({}^4F)$ transition. The two peaks A and B connected with this transition for CdTe: Co are shown in Fig. 10. The peak A we interpret as a transition to two components G and $E_{5/2}$ of the ${}^4T_1({}^4F)$ level, whose splitting should be very small as predicted by a crystal field theory. The peak B is connected with a transition to the $G(-3/2 \mid \lambda \mid)$ level. Similar peaks to A and B are found in ZnTe: Co. They are shown in Fig. 11. The interpretation is exactly the same as for CdTe: Co. Besides these two peaks A and B, a third one C appears for GaP: Co and GaAs: Co. This one could be due to the transition to the fourth component $E_{1/2}$ of the ${}^4T_1({}^4F)$ level. This assignment leads to anomalous large spin-orbit splitting of the ${}^4T_1({}^4F)$ level - larger than free ion spin-orbit splitting. This was observed also for some II-VI compounds (1, 4). The cause of this effect is not known. Table II gives the energy of the transitions and the values of B and Dq deduced from them. In GaAs: Co probably the breakdown of the crystal field approach is observed. No set of values of B, Dq and λ fit the spectrum.

It is also possible that our fit to the split ${}^4T_1({}^4F)$ level is not a correct one. M. A. Weakliem [Ref. 4] observed that the separation between G and $E_{5/2}$ is much higher than predicted by a crystal field theory. The peak A can be connected with the G component and the peak B with the $E_{5/2}$ one, and the peak C with $G(-3/2 \mid \lambda \mid)$ component of the ${}^4T_1({}^4F)$ level. This assignment will shift the position of the ${}^4T_1({}^4F)$ level further into the infrared between B and C peaks. In this case we can explain the spectrum of GaAs: Co within the framework of the crystal field theory. The value $B \approx 300 \text{ cm}^{-1}$ and $Dq \approx 470 \text{ cm}^{-1}$ will fit the spectrum. Consequently, this approach will also give the different values of B and Dq for cobalt in GaP. The value $B \approx 450 \text{ cm}^{-1}$ and $Dq \approx 420 \text{ cm}^{-1}$ will fit the spectrum of GaP: Co. These values are in better agreement with the values for B and Dq for nickel in GaP. Without additional experiments it is not possible to decide which of these two explanations is the correct one.

REFERENCES

1. R. Pappalardo and R. E. Dietz, Phys. Rev., 123, 1182 (1962).
2. W. Low and M. Weger, Phys. Rev., 118, 1119 (1960).
3. L. E. Orgel, An Introduction to Transition Metal Chemistry, London: Methuen & Co., LTD; New York: John Wiley & Sons, Inc.
4. H. A. Weakliem, Journal of Chemical Physics, 36, 2117 (1962).
5. Y. Tanabe and S. Sugano, J. Phys. Soc. (Japan) 9, 753, 766 (1954).
6. D. M. Loeschner, J. W. Allen, G. L. Pearson, Proc. of the Internatl. Conf. on the Physics of Semiconductors, Kyoto, 1966

FIGURE CAPTIONS

- Fig. 1 The splitting of the ground state 5E by spin-orbit coupling of the second order and by the axial field b in the $\langle 111 \rangle$ direction calculated for $Dq = 282 \text{ cm}^{-1}$ and $\lambda = -95 \text{ cm}^{-1}$. The fit with observed peaks is indicated by arrows.
- Fig. 2 Absorption spectrum of CdS: Fe at liquid helium temperature.
- Fig. 3 CdS: Fe expanded absorption in the 2550 cm^{-1} region.
- Fig. 4 Absorption spectrum of GaAs: Fe at liquid helium temperature.
- Fig. 5 Absorption spectrum of GaP: Ni at liquid helium temperature.
- Fig. 6 Energy level diagram for states of the d^8 configuration in a crystal field of tetrahedral symmetry.
- Fig. 7 GaP: Ni expanded absorption in the 1μ region at liquid helium temperature.
- Fig. 8 Energy level diagram for states of the d^7 configuration in a crystal field of tetrahedral symmetry.
- Fig. 9 CdTe: Co Expanded absorption connected with the transition $^4A_2(^4F) \rightarrow ^4T_1(^4P)$ at liquid helium temperature.
- Fig. 10 CdTe: Co absorption connected with the transition $^4A_2(^4F) \rightarrow ^4T_1(^4F)$ at liquid helium temperature.
- Fig. 11 Absorption spectrum of ZnTe: Co at liquid helium temperature.
- Fig. 12 Absorption spectrum of GaP: Co at liquid helium temperature.
- Fig. 13 GaP: Co expanded absorption connected with the transition $^4A_2(^4F) \rightarrow ^4T_1(^4P)$ at liquid helium temperature.
- Fig. 14 Absorption spectrum of GaAs: Co at liquid helium temperature.
- Fig. 15 GaAs: Co expanded absorption connected with the transition $^4A_2(^4F) \rightarrow ^4T_1(^4P)$ at liquid helium temperature.

TABLE I

The spin-orbit coupling parameter λ obtained from the spectra and width of the absorption band connected with the transition $^5E \rightarrow ^5T$.

	$ \lambda $ [cm ⁻¹]	Width of the absorption band connected with transition $^5E \rightarrow ^5T$
CdTe	50	580 cm ⁻¹
ZnTe	50	530 cm ⁻¹
ZnSe	88	780 cm ⁻¹
CdS	95	1000 cm ⁻¹
GaP	87	750 cm ⁻¹
GaAs	86	1000 cm ⁻¹

TABLE II

Position of the $^4T_1(^4F)$ and $^4T_1(^4P)$ levels as deduced from them the crystal field parameters B and Dq for measured semiconductors.

Host	$^4A_2(^4F)$	$^4T_1(^4F)$	$^4T_1(^4P)$	B[cm ⁻¹]	Dq[cm ⁻¹]
CdTe	0	5400cm ⁻¹	11150cm ⁻¹	485	315
ZnTe	0	5100cm ⁻¹	11050cm ⁻¹	460	335
GaP	0	7900cm ⁻¹	12300cm ⁻¹	290	540
GaAs	0	8100cm ⁻¹	11400cm ⁻¹		

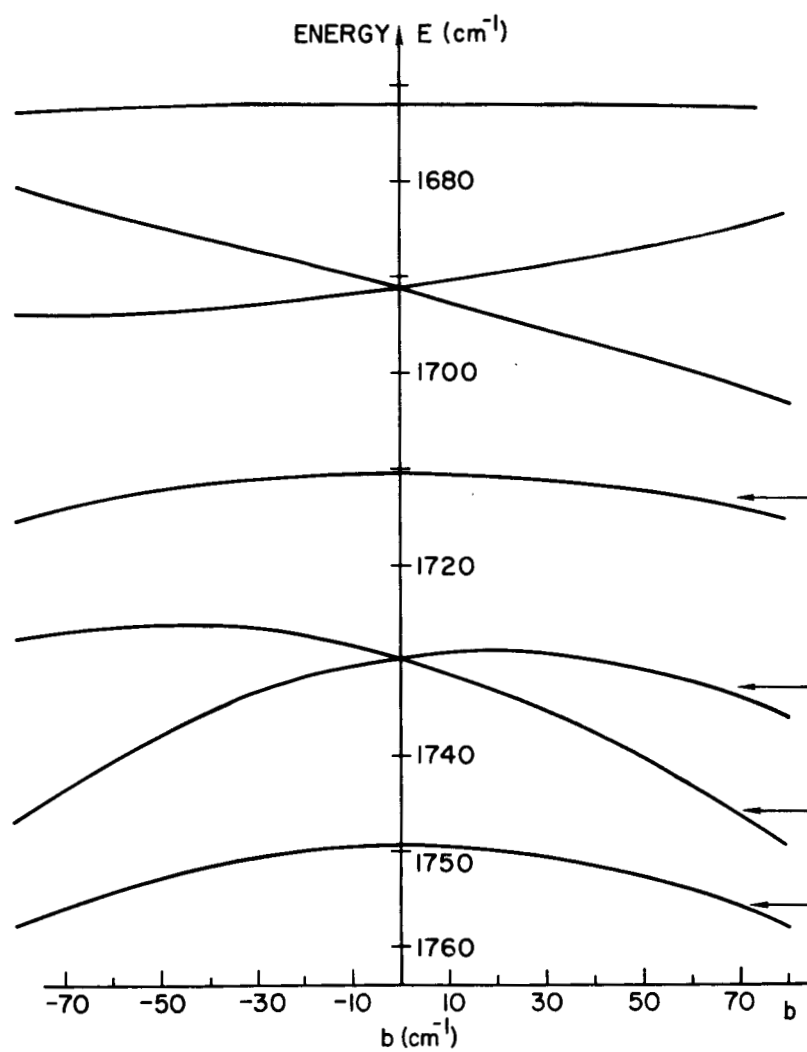


FIGURE 1

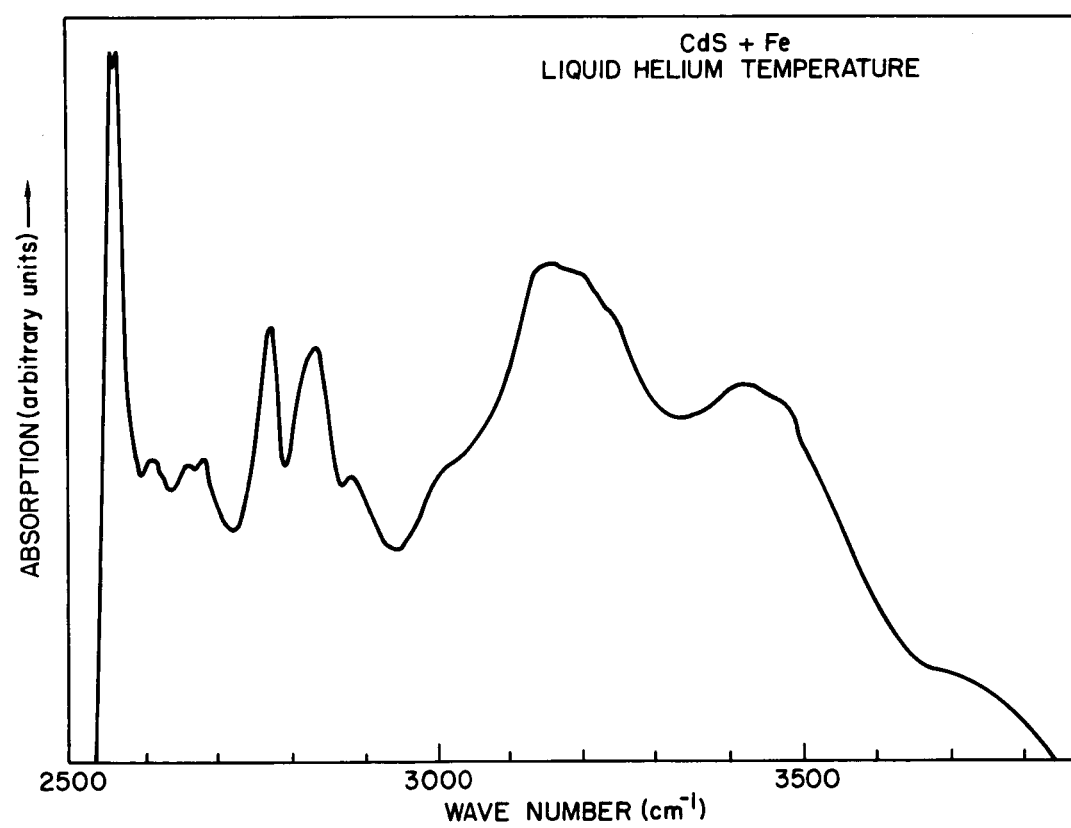


FIGURE 2

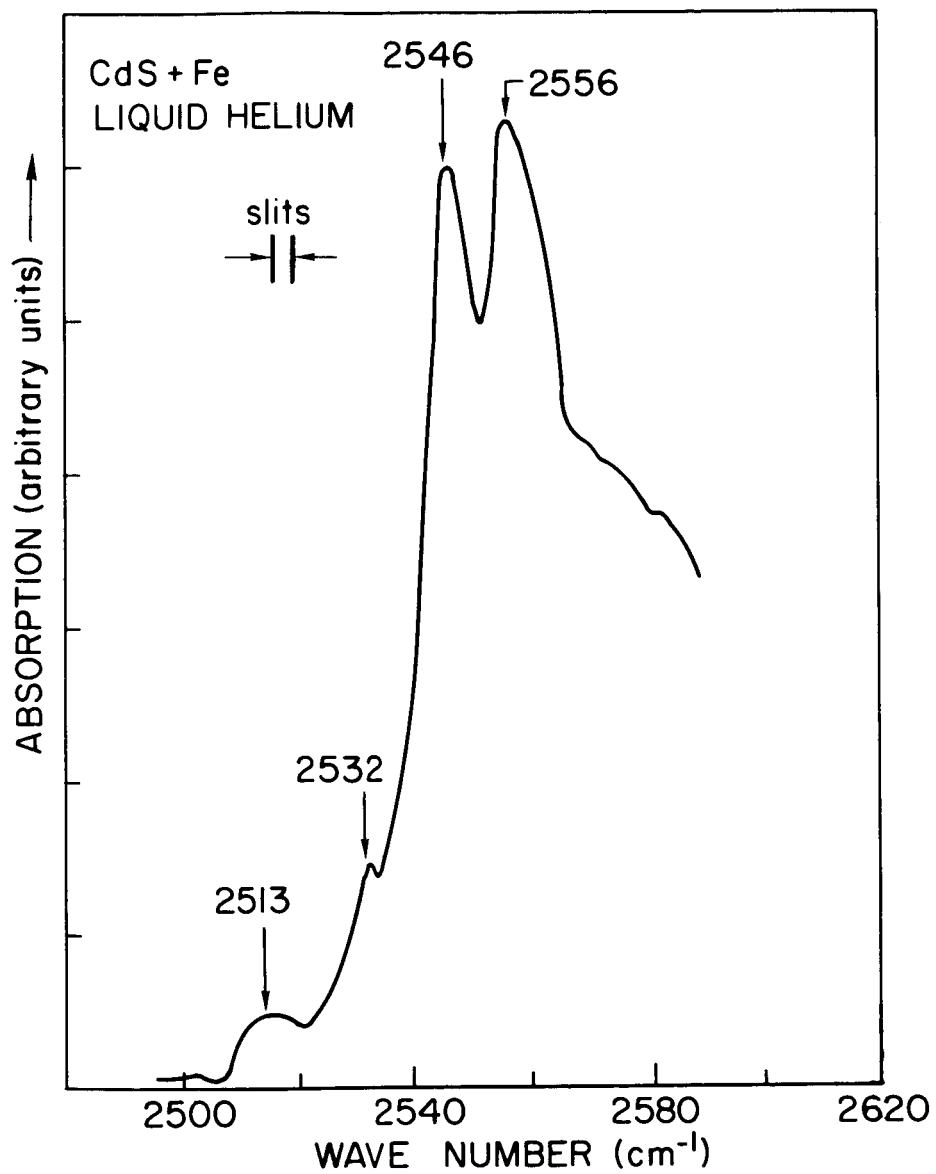


FIGURE 3

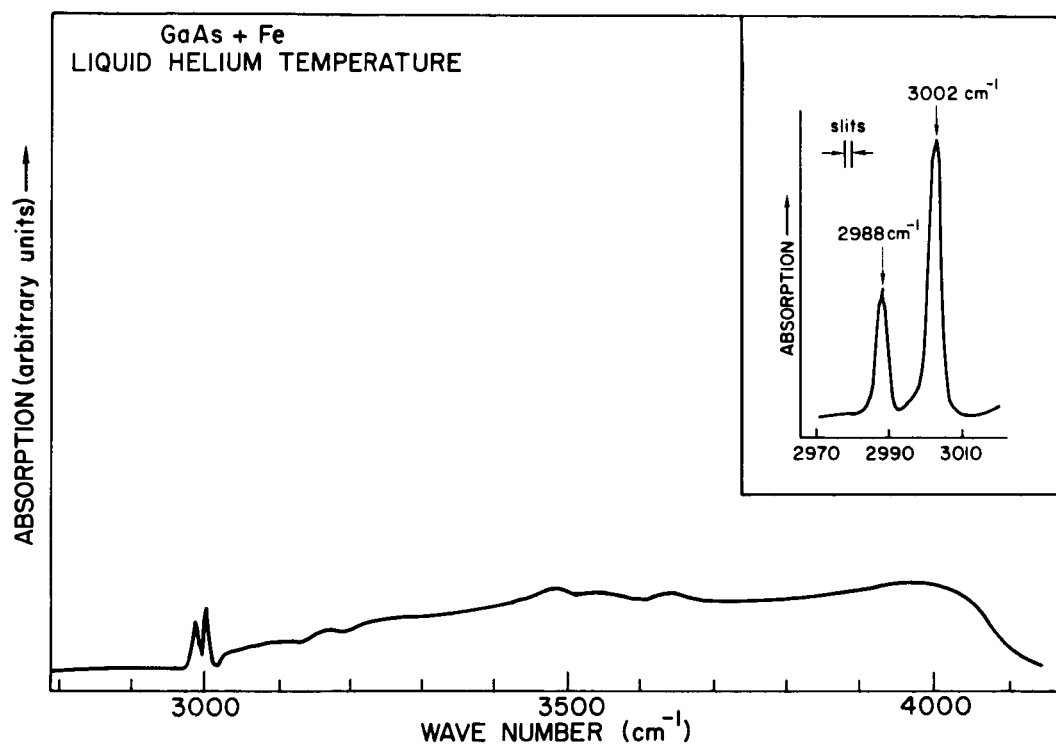


FIGURE 4

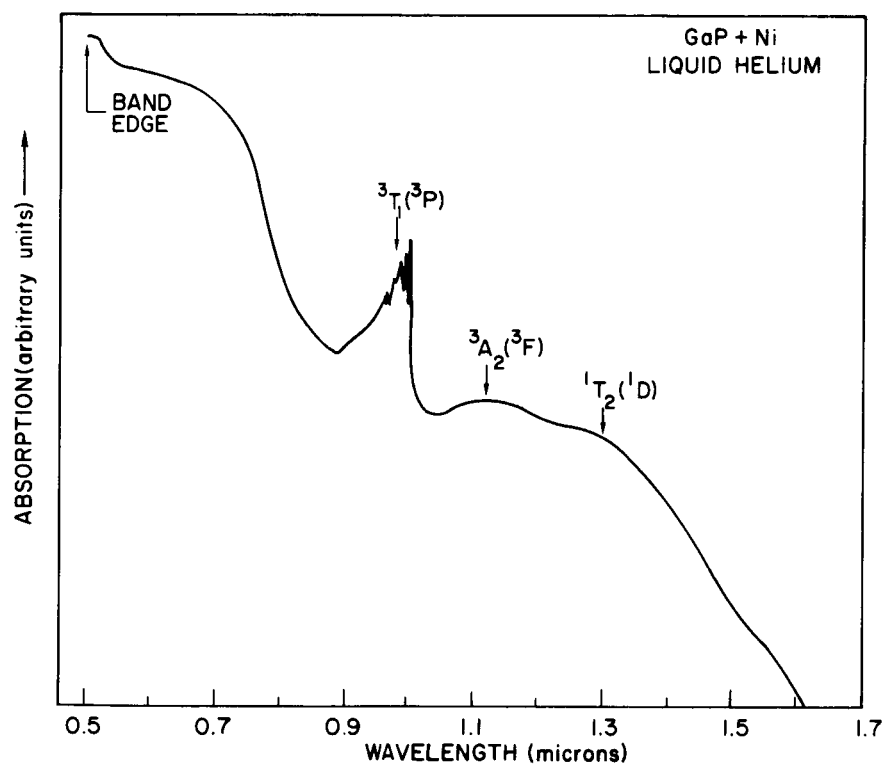


FIGURE 5

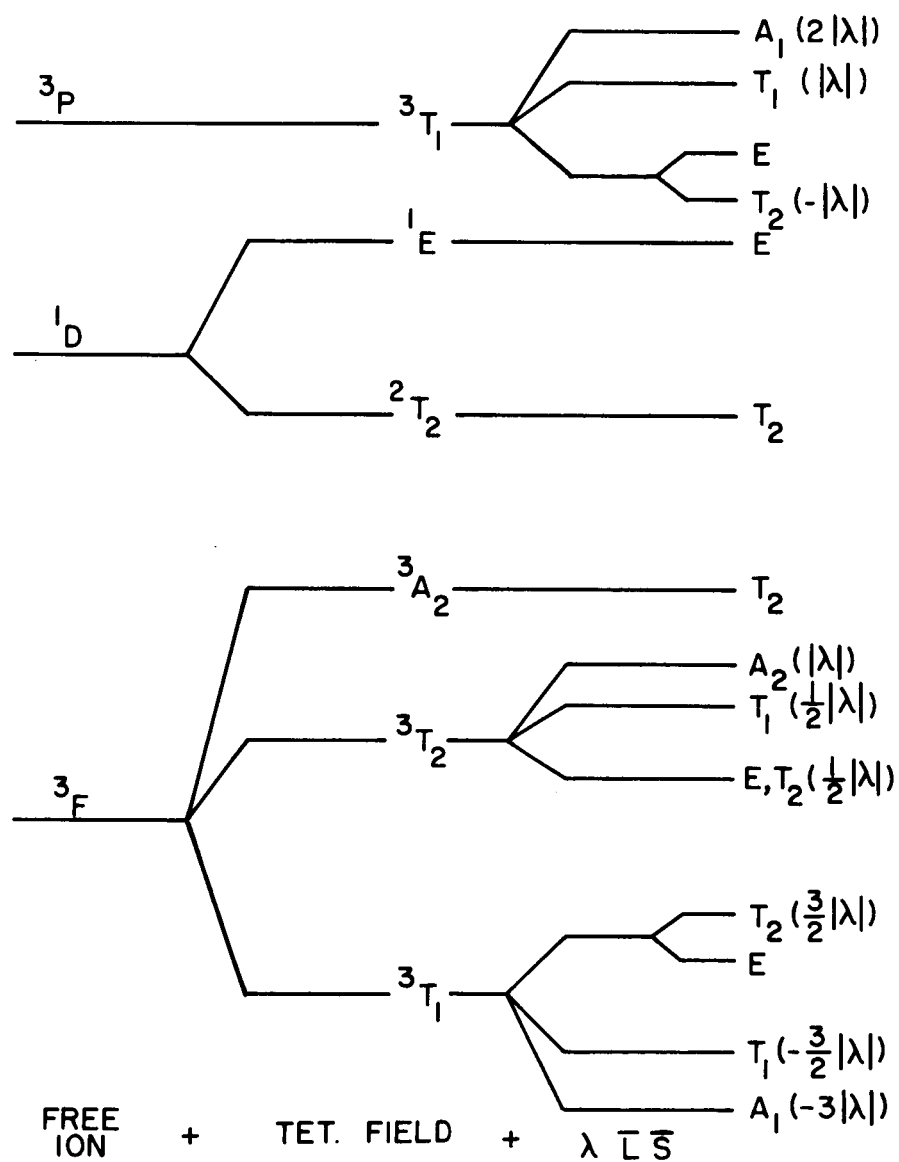


FIGURE 6

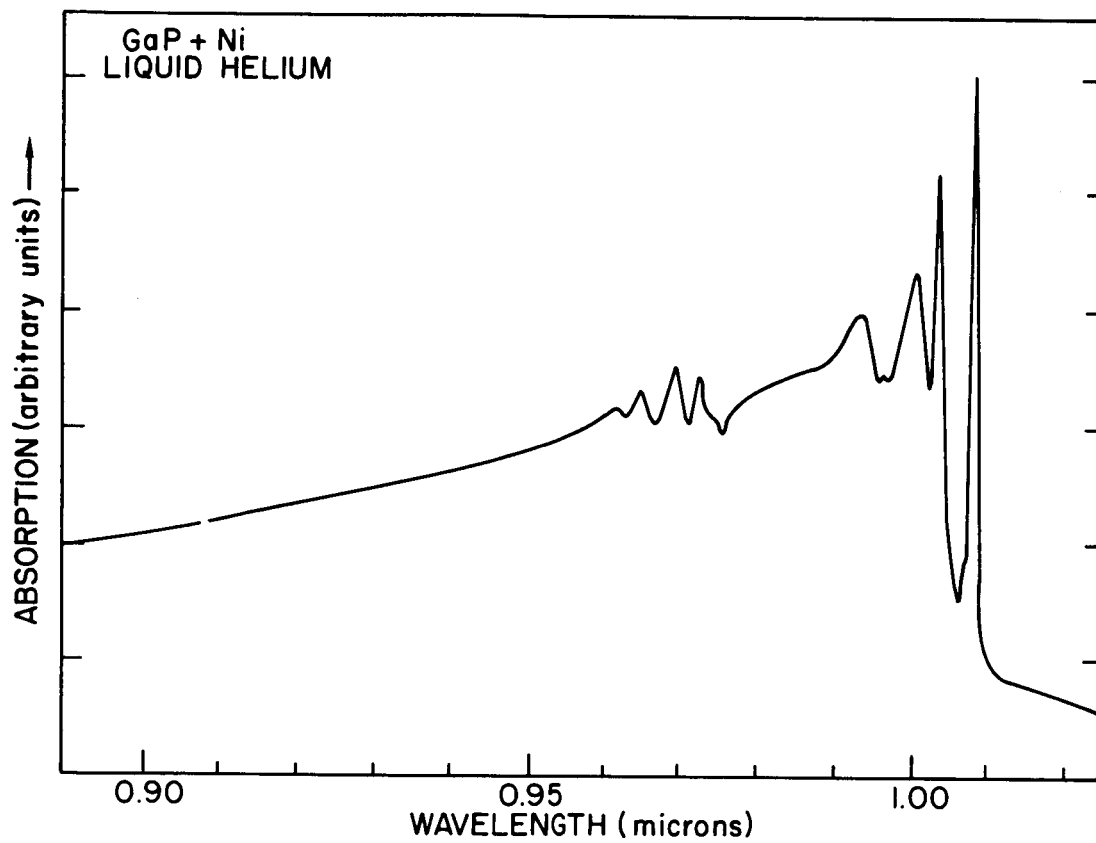


FIGURE 7

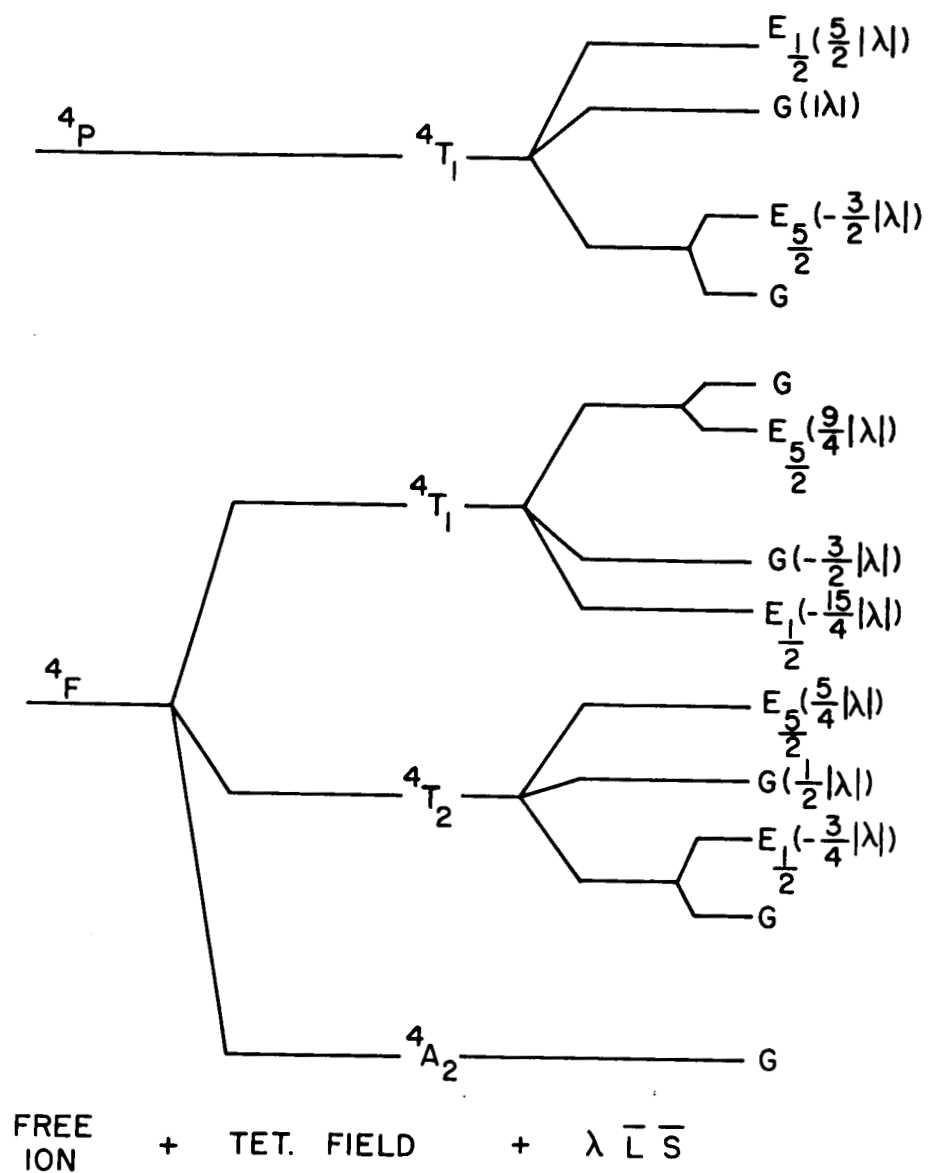


FIGURE 8

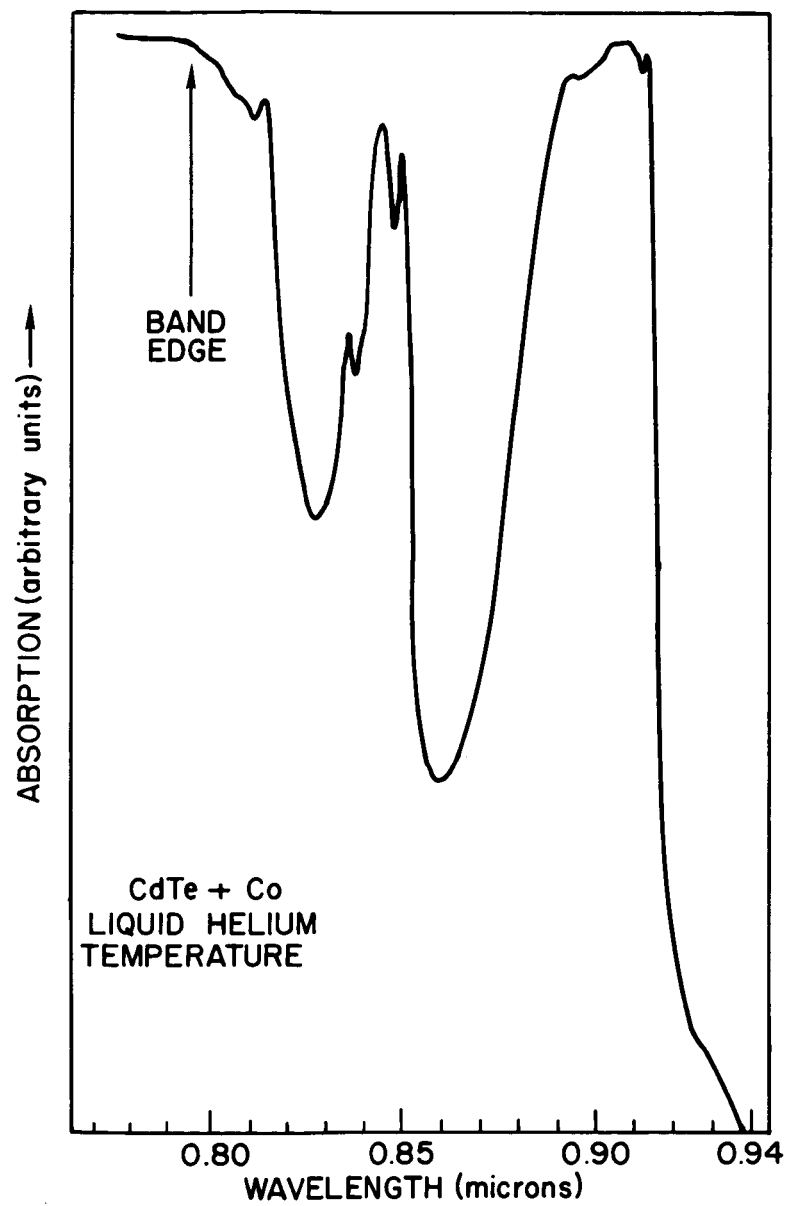


FIGURE 9

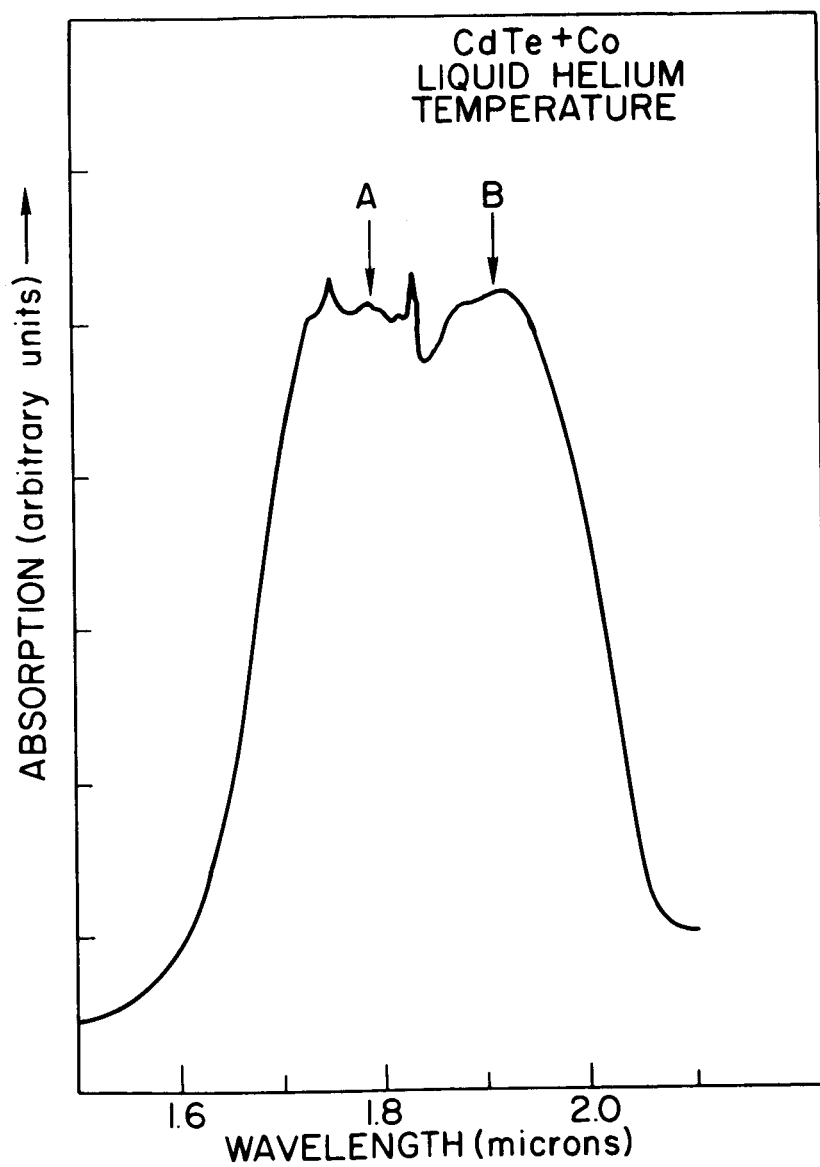


FIGURE 10

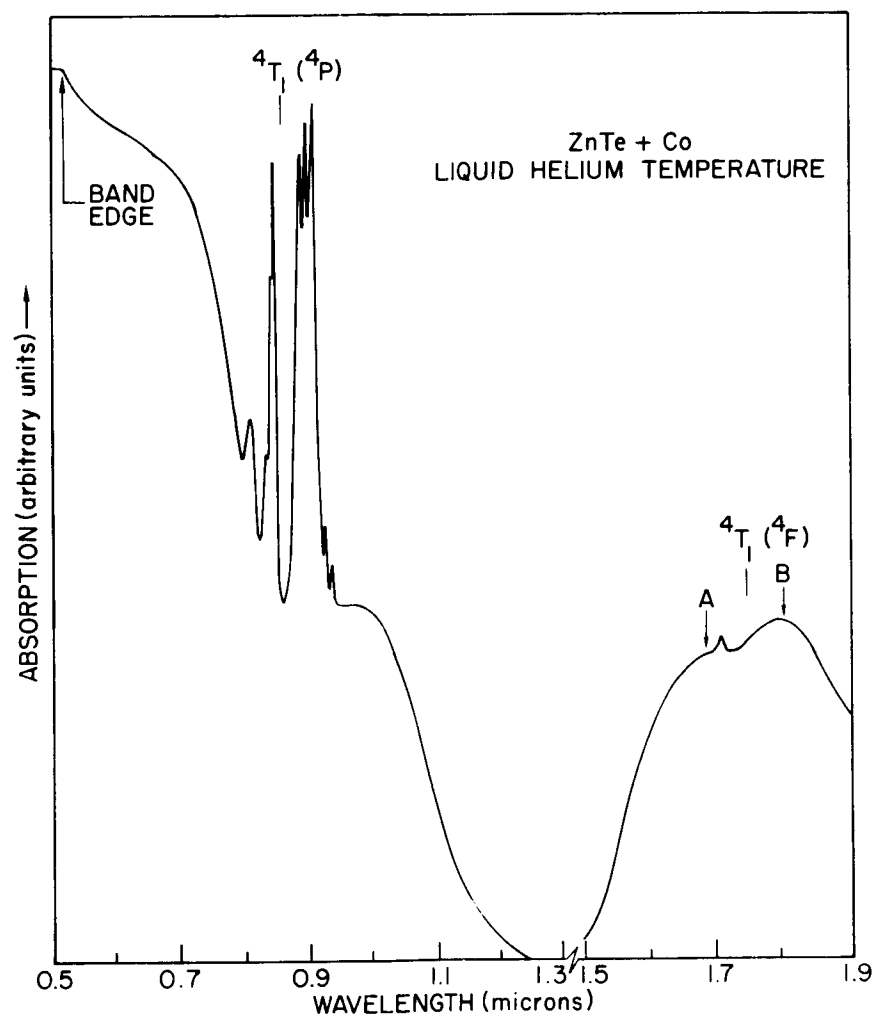


FIGURE 11

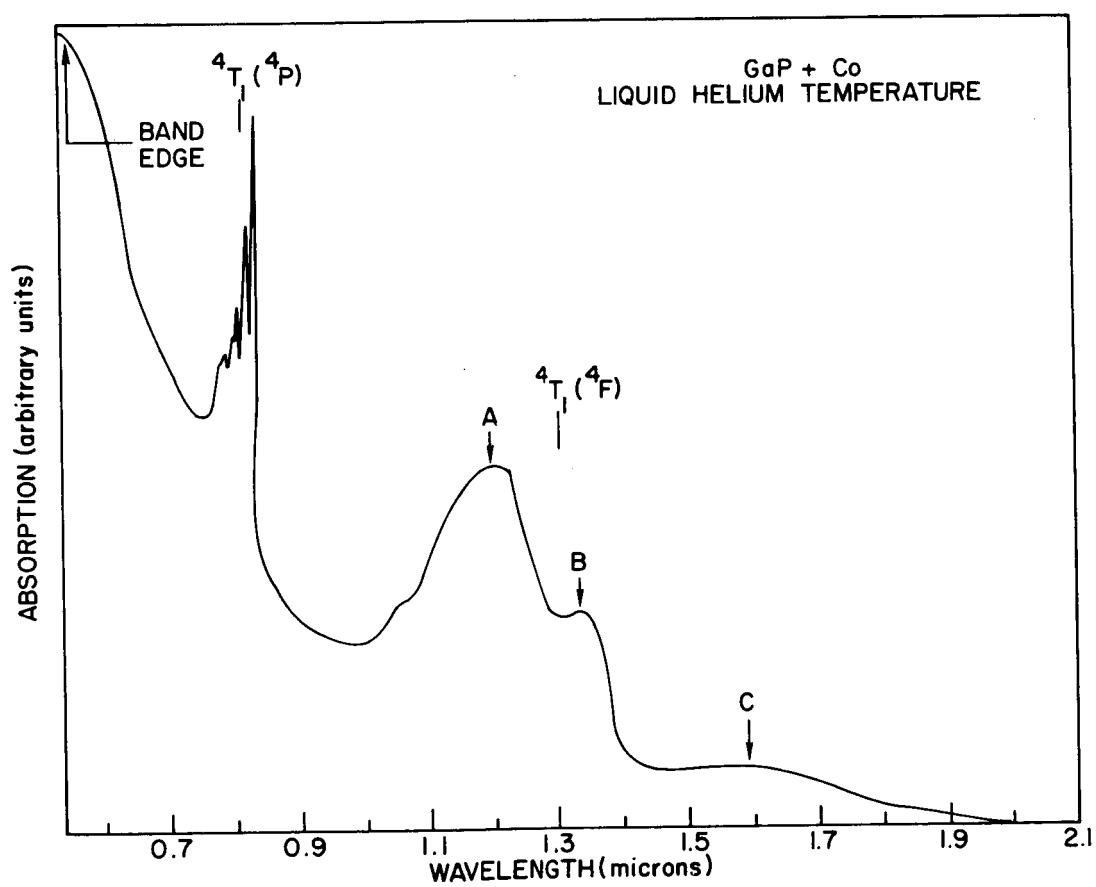


FIGURE 12

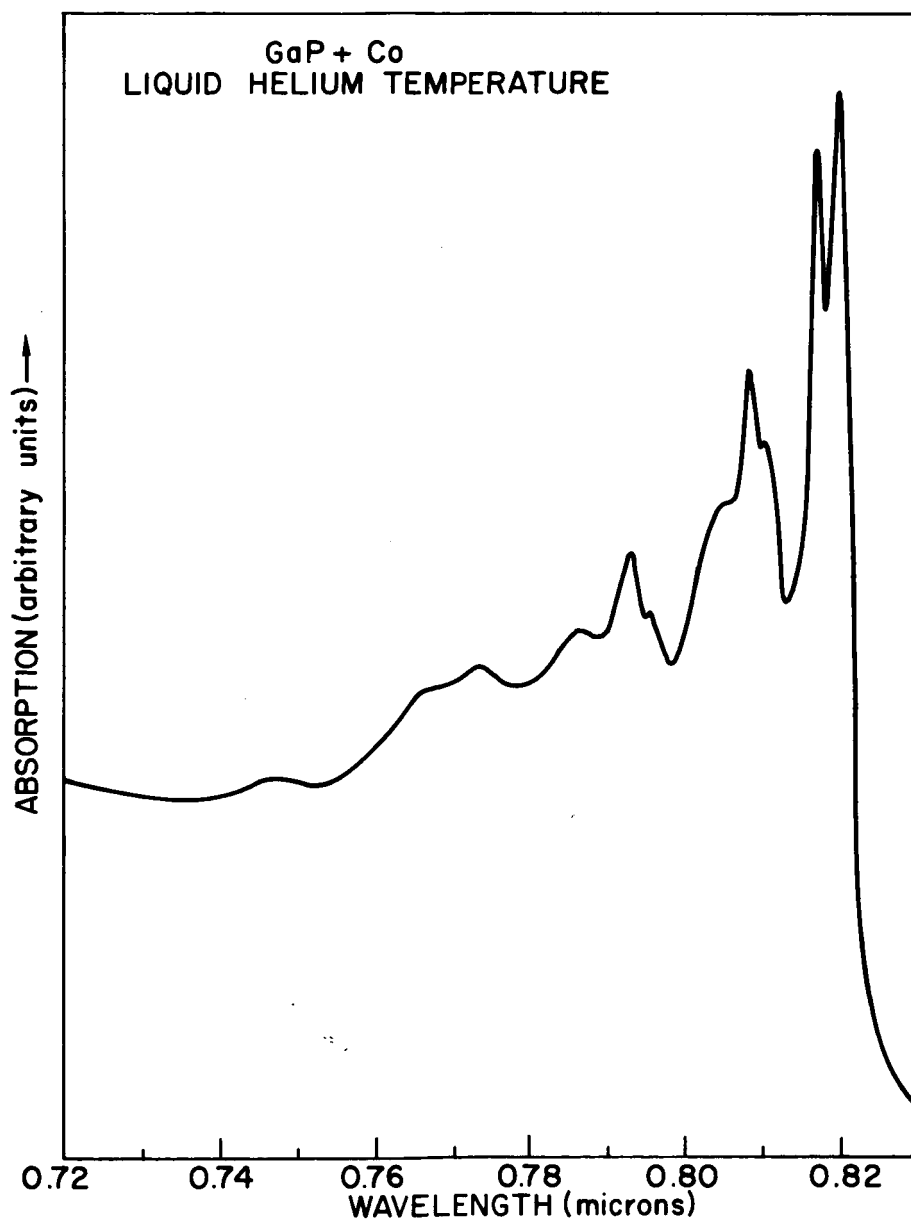


FIGURE 13

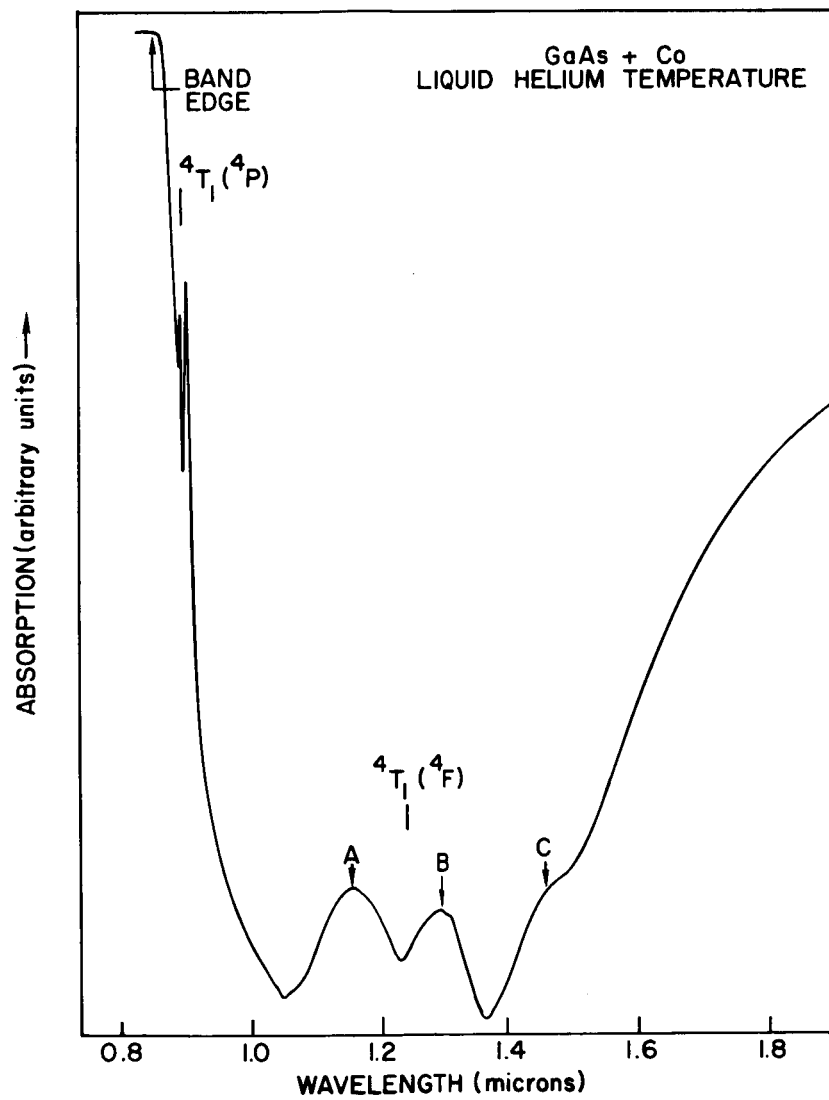


FIGURE 14

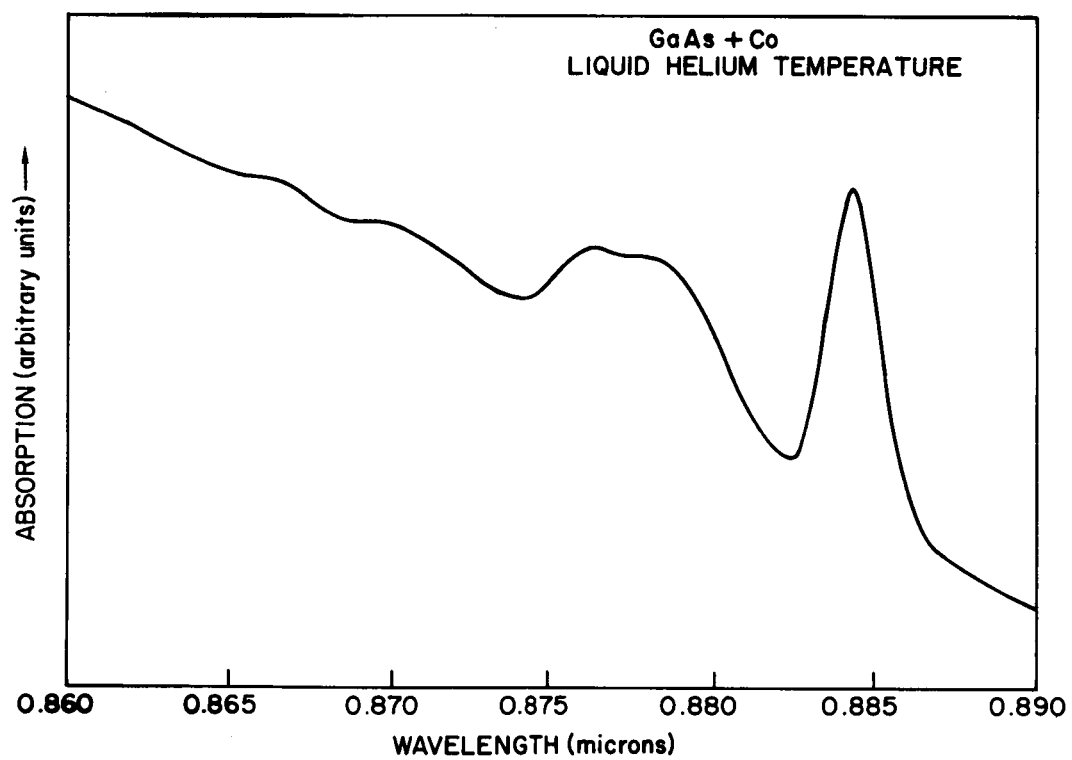


FIGURE 15

PROJECT 5112: THE PROPERTIES OF RECTIFYING JUNCTIONS IN $\text{GaAs}_x\text{P}_{1-x}$

National Aeronautics and Space Administration

Grant NsG 555

Project Leader: G. L. Pearson

Staff: S. F. Nygren*

The purpose of this project is to study the preparation and characterization of rectifying junctions in GaP and $\text{GaAs}_x\text{P}_{1-x}$. In particular, we wish to relate the structure of the crystals to the electrical properties of the junctions. This quarter our study of imperfections in single crystals of gallium phosphide has been continued. Crystals have been studied with the optical microscope, with some new chemical etchants, and with Lang topography.

A. Observation with an Optical Microscope.

A polished crystal of GaP appears quite homogeneous to the naked eye. It looks much like a piece of orange colored glass. When such a crystal is examined in an optical microscope, however, small imperfections may often be found. To examine these defects, a crystal has been observed in an optical microscope with transmitted light. When a defect was located, several photographs were taken. All photographs were taken without moving the crystal, except that each photograph was focused at a different depth inside the crystal. The crystal was then etched in our usual dislocation etchant ($8\text{g K}_3\text{Fe}(\text{CN})_6$: 12g KOH : $100\text{g H}_2\text{O}$), and a final picture was taken of the etch pattern.

The information from the photographs can be used to determine the locus of the defect. It turns out to be a line that

* NSF Fellow

lies in one of the $\{111\}$ planes that intersects the surface at an angle of $70^{\circ} 32'$. To define a coordinate system, call the surface (111) , and the plane of the defect $(\bar{1}\bar{1}1)$. Then the defect line is running in the $[112]$ direction and lying in the $(\bar{1}\bar{1}1)$ plane.

The line of the defect emerges from the crystal about midway between two etch pits that are $7\mu\text{m}$ apart. The point of emergence itself, however, is not marked by an etch pit. As yet, the exact nature of this line defect is not known.

B. Etching.

The dominant imperfections in the GaP crystals grown at this laboratory are two dimensional defects that are parallel to $\{111\}$ planes. Our usual dislocation etchant reveals these defects by making grooves where these defects intersect the $\{111\}\text{Ga}$ surfaces of the crystals. To see if other chemicals will mark these defects differently, the effects of several other common etchants have been examined. These etchants are listed in Table I, and their effects are summarized there.

Etchants #7 and #8 are of special interest. Both of them appear to be good dislocation etchants. Etchant #7 makes etch grooves similar to the ones made by our usual etchant: All of the grooves have smooth bottoms. On the other hand, some of the grooves produced by etchant #8 have pits at random intervals along their bottoms. This is the first evidence to suggest that the grooves may actually be rows of etch pits that are so close together that individual pits cannot be resolved. This would indicate sets of parallel, very closely spaced dislocations.

Etchants #1 and #2 are also of interest since they polish the {111}P faces of the crystals. This property may make them useful for thinning GaP crystals by the jet technique described by Booker and Stickler [Ref. 1]. Initial efforts to use the jet technique have revealed two difficulties: First, the etch grooves tend to appear on the {111}P faces so that the polish is not perfect. Second, if the surface formed by the jet action becomes too concave, pits tend to form. However, if these difficulties can be overcome, and if a suitable method for polishing the {111}Ga face of GaP can be found, it will be possible to prepare samples that can be observed in the transmission electron microscope. An electron microscope examination of GaP would reveal the defect structures easily and with great resolution.

C. Lang Topography.

In the previous quarterly report [Ref. 2] it was observed that x-ray topography [Ref. 3] is difficult to perform in epitaxial GaP because there are so many dislocations and so much strain in such GaP. The images of all the various strain fields overlap, and no distinct images can be resolved. To reduce this difficulty, the crystal thickness was reduced to about 100 μ m. Also, the crystal was etched to reveal dislocations, and finally it was annealed in vacuum at 350 $^{\circ}$ C for one hour; the annealing process is known to remove strain caused by surface damage from silicon [Ref. 4].

Two topographs of the crystal were taken, one before etching and one after annealing. Both used reflections from {110} planes, and both exposures were for four hours. The topograph taken before

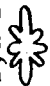
annealing revealed a few imperfections, but most of the picture was obscured. The topograph taken after annealing was noticeably better although there were still many clouded areas. This is interesting since the strain patterns revealed by birefringence are not noticeably changed by annealing.

Many line defects are revealed by the topograph that was taken after annealing. They all run in $\langle 110 \rangle$ directions, and they correspond to the grooves made by etching. The topograph also revealed that the sample contained a subgrain boundary or something similar, since not all of the sample produced a picture that was in contrast.

Crystal preparation procedures must be improved before much more information can be learned from the Lang topography technique. However, once the technique is perfected, it will allow resolution of dislocations (if they are not too dense), stacking faults, and twins.

REFERENCES

1. G. R. Booker and R. Stickler, Brit. J. Appl. Phys., 13, 446 (1962).
2. S. F. Nygren, Quarterly Progress Report for period July 1 - September 30, 1966.
3. A. R. Lang, J. Appl. Phys., 29 (1958).
4. W. Kleinfelder, private communication.

TABLE I Etchants for GaP			
Etchant*	Time sample is immersed	Effect on {111} Ga Face	Effect on {111} P face
1a. 10 HCl: 1 H ₂ O**	5 min	irregularly shaped meses, deep grooves	polished, but lumpy
1b. 20 HCl: 7 H ₂ O**	5 min	big, deep pits and grooves	polished
1c. 10 HCl: 6 H ₂ O**	1 min	deep pits and grooves	polished
2. 1 HCl: 1 HNO ₃	10 min	rough and grainy	polished with a few short grooves
3a. Bromine	10 min	little or no effect	grainy
3b. 1 Br: 1 Benzene	2 min	little or not effect	grainy
3c. 1 Br: 2 Benzene	2 min	short, shallow grooves	grainy
3d. 1 Br: 3 Benzene	2 min	grooves	small pits
3e. 1 Br: 50 Benzene	10 min	little or no effect	grainy
4. 1 H ₂ SO ₄ : H ₂ O**	10 min	grooves, irregular snowflake-like pits	rough and grainy
5. CP-4	10 min	Large, shallow football-shaped pits, grooves rectangular pits	grainy
6. 1 HNO ₃ : 1 HF	10 min	grooves, a few pits shaped like 	grainy
7. 2 H ₂ O ₂ : 1 HF	10 min	grooves, dislocation-like patterns	pitted
8. methanol saturated with iodine, plus a few drops of Br	1 hour	dislocation-like patterns	little or no effect

*All etchants are fresh.

**Used hot. Temperature increase is produced by heat of mixing.

PROJECT 5116: DONOR IMPURITIES IN GaP

National Aeronautics and Space Administration
Grant NSG-555

Principal Investigator: G. L. Pearson
Staff: A. Young*

The purpose of this project is to study the behavior of shallow donors in gallium phosphide. In particular S, Se, and Te will be diffused into GaP to determine solubilities and diffusion parameters. This information will be useful in delineating the properties of GaP doped with these shallow donor impurities.

Crystal Growth

During the past quarter, three more gallium phosphide crystals were grown by the open-tube epitaxial method developed at this laboratory. These crystals were characterized by very smooth and shiny growth (111 gallium) faces, and by the complete absence of the GaAs seed after growth. The principal differences in growth conditions from previous runs were a 10% lower hydrogen flow through the PCl_3 bubbler (45 cc/min) with total flow kept constant (150 cc/min), and a lower temperature for the gallium source (928°C instead of the previous $950-970^\circ\text{C}$).

Preliminary electrical measurements of one of the crystals, however, indicate an extremely low Hall mobility of approximately $10 \text{ cm}^2/\text{v-sec}$ (resistivity was 50 ohm-cm). Since the cleavage of the crystals seem to indicate single-crystal material, this low mobility may be due to poor alloyed contacts, or to the presence of compensating impurities.

* NSF Fellow

RADIOTRACER CONSIDERATIONS

The specific activity of the radiotracer to be used in an experiment is determined by several factors.

1) The activity must be sufficiently above the background count to give the required accuracy.

2) The activity must not be so high as to cause overloading of the counter, or to pose a serious health or safety hazard.

The relation between experimental quantities such as radioactive counts per minute (CPM) and sample size, and the parameters we wish to determine, such as solubility of an impurity in a host lattice, is given by:

$$\text{CPM} = \eta \text{ DPM} = \eta \quad a(\text{mc/mg}) \times C(\text{atoms/cm}^3) \times \text{At.Wt.} \times \text{Vol.}(\text{cm}^3) \\ \times 3.69 \times 10^{-12}$$

where CPM = counts per minute from a sample as indicated by a particular counter

DPM = atomic disintegrations per minute in the sample

η = counting efficiency = the ratio between the actual number of disintegrations and the registered counts; a combination of geometrical factors and the energy of radiation being counted.

a = specific activity of the impurity being used, in millicuries per milligram

C = concentration of impurities in the sample being measured

At.Wt. = atomic weight of impurity

Vol. = volume of sample being measured

The formula above can be used to solve for the approximate activity of radiotracer needed. Suppose we ask for a 10% count-

ing accuracy when a background count of 20/minute exists. This requires 200 cpm from the sample itself. For a sample size with an 0.2" disc, an incremental lap of 2.5 microns, a concentration of $10^{19}/\text{cm}^3$, and specific activity of sulfur-35 impurity of 1 mc/mg, the CPM registered will be approximately 300. For counting efficiency, the value 5×10^{-3} has been used as determined from an independent experiment with a commercial carbon-14 standard (which has a beta energy approximately the same as that of the sulfur-35) in the Baird Atomic Proportional Counting Chamber.

Sulfur-35 of high specific activity (1 mc/mg) has been ordered and will be available next quarter for further work.

Radioactive Diffusions

Radioactive sulfur-35 has been diffused into single-crystal GaP samples in the presence of phosphorus vapor to determine diffusion times and temperatures required in future experiments. Diffusion profiles have been obtained using standard lapping techniques. A calibration standard made from the same benzene-sulfur solution used in the diffusion experiments permits an absolute determination of sulfur solubilities in GaP.

Experimental Procedure

Gallium phosphide samples are lapped, mechanically polished, cleaned in the ultrasonic cleaner, degreased, and stored in methanol. The quartz ampoules used are "torched out" under vacuum for approximately 10 minutes.

Next, the radioactive sulfur in benzene solution is pipetted into the ampoule, and the benzene evaporated by passing a

stream of dry nitrogen over the liquid while heating the benzene vapor with an infrared lamp or a heating tape.

The desired amount of phosphorus is placed in the ampoule along with the GaP sample. The ampoule is sealed at a vacuum of about 10^{-3} torr. Since sulfur is quite volatile, it is desirable to seal the ampoule as quickly as possible with a minimum of heat. Wrapping a wet asbestos pad around the ampoule is helpful in keeping the sulfur cool.

After diffusion, the ampoules are quenched in water. The samples are weighed to evaluate any weight loss that may have occurred. Before lapping to obtain the diffusion profile, the samples are boiled in benzene to remove any excess sulfur that may have condensed during quenching. Circular discs 0.2" in diameter are cut out with an ultrasonic tool to eliminate edge diffusion.

The diffusion profiles and important parameters of the two radiotracer diffusions done this quarter are given in Figs. 1 and 2 and in Table I. The diffusion conditions are essentially the same except that diffusion R-2 is at 1200°C for 24 hours, and R-3 is at 1150°C for 48 hours. The numbers given should be taken as approximate only, since no particular care was taken, for example, in measuring ampoule volumes, and graphical interpolations were made in obtaining vapor pressures.

The results obtained for diffusion constant and solubility of sulfur in GaP are summarized in Table II. These were obtained by a least-squares fit of the complementary error function to the experimental points. Since the activity of the sulfur-35 was

quite low (about 50 microcuries/mg), counting errors were rather large.

Several experimental difficulties should perhaps be mentioned here briefly. One is the error introduced by "wedging" during lapping of the samples after diffusion. The effect of this error is to introduce uncertainty as to the true solubilities, since the diffusion fronts and the lapped surface are no longer parallel. This error can be accounted for to some extent in the manner discussed by Shirn, Wadja, and Huntington.¹

Use of a rubber pad mounted on the aluminum lapping button along with the samples was very successful in eliminating the wedging when a silicon sample was used. However, attempts to use this method with gallium phosphide samples were not as successful as the samples cracked while being lapped. Use of a harder rubber pad may prove to be beneficial.

A second experimental consideration is the surface deterioration of the sample. In the diffusions done this quarter with full size (1/4" square) samples, the following observations were made:

The "equivalent surface loss" for these samples was less than that observed for the much smaller samples for which preliminary results were reported last quarter.

However, one face of the samples was quite rough, and data from this side gave meaningless results. The second face was generally quite smooth and shiny. Data from this side was used in obtaining the results reported earlier in this report.

Summary

In summary, several diffusions have been made with radiotracer sulfur-35 in order to obtain estimates of diffusion coefficients and impurity solubilities as an aid in future diffusion experiments. The diffusion coefficients obtained were quite small, in the range 10^{-11} to 10^{-12} cm²/sec, as is generally found for substitutional-type diffusion mechanisms. Several experimental difficulties - the low specific activity of the tracer used, wedging in the lapping process, and surface deterioration should be considered when results are examined. Higher specific activity (1 mc/mg) sulfur has been ordered which should enable shorter diffusion times and consequent lessening of surface deterioration.

Several goals for next quarter will be - work on the reproducibility of results, time dependence of the apparent surface concentration (solubility), and constancy of the vapor pressures in the ampoule during diffusion.

REFERENCES

1. G. A. Shirn, C. S. Wadja, H. B. Huntington, Acta. Met., 1, 513 (1953).

FIGURE CAPTIONS

Figure 1 - Diffusion profile of sulfur in GaP crystal R-2. Vertical lines indicate standard deviation.

Figure 2 - Diffusion profile of sulfur in GaP crystal R-3.

Table I - Diffusion Parameters

Diffussion	R-2	R-3
Diffusion Temp.	1201°C	1143°C
Diffusion Time	24 hours	48 hours
Ampoule Volume	1.48 ml.	1.48 ml.
Wt. GaP(before diffusion)	67.155 mg.	29.529 mg.
Wt. GaP(after diffusion)	66.661 mg.	29.284 mg.
Wt. Loss	0.494 mg.	0.245 mg.
% Wt. Loss	0.75%	0.85%
Equivalent Surface Loss	3 microns	1.5 microns
Wt. Sulfur	15 micrograms	15 micrograms
Sulfur Density	10 micrograms/ml.	10 micrograms/ml.
S ₂ Pressure	1.8×10^{-2} ATM*	1.7×10^{-2} ATM*
Wt. Phosphorus	685 micrograms	649 micrograms
Phosphorus Density	464 micrograms/ml.	444 micrograms/ml.
P ₂ Pressure	4×10^{-1} ATM	3.8×10^{-1} ATM
P ₄ Pressure	1.9×10^{-1} ATM	1.8×10^{-1} ATM
Sample Thickness	15 mils	7 mils
Vacuum	5×10^{-3} torr	5×10^{-3} torr

* Analysis of the amount of sulfur in the GaP after diffusion was significant in relation to the total amount placed in the ampoule. Thus the sulfur vapor pressure changed during diffusion (by a factor of 2 or more).

Table II
Diffusion Constant (D) and Surface Concentration(N_s) of Sulfur in
Gallium Phosphide* (Preliminary Only).

Diffusion	Temperature	$D(\text{cm}^2/\text{-sec})$	$N_s(\text{cm}^{-3})$
R-2	1201°C	1.2×10^{-11}	1.2×10^{20}
R-3	1143°C	4×10^{-12} **	2.1×10^{20} **
		1.3×10^{-12} ***	3.7×10^{20} ***

* Diffusion conditions given in Table I.

** Using only 5 points on diffusion profile.

*** Using all 7 points on diffusion profile.
The present program fits a curve through.
[sulfur concentration] vs. x whereas it should
really make a least squares fit of.
log [sulfur concentration] vs. x in order not
to weight errors near the surface so heavily.

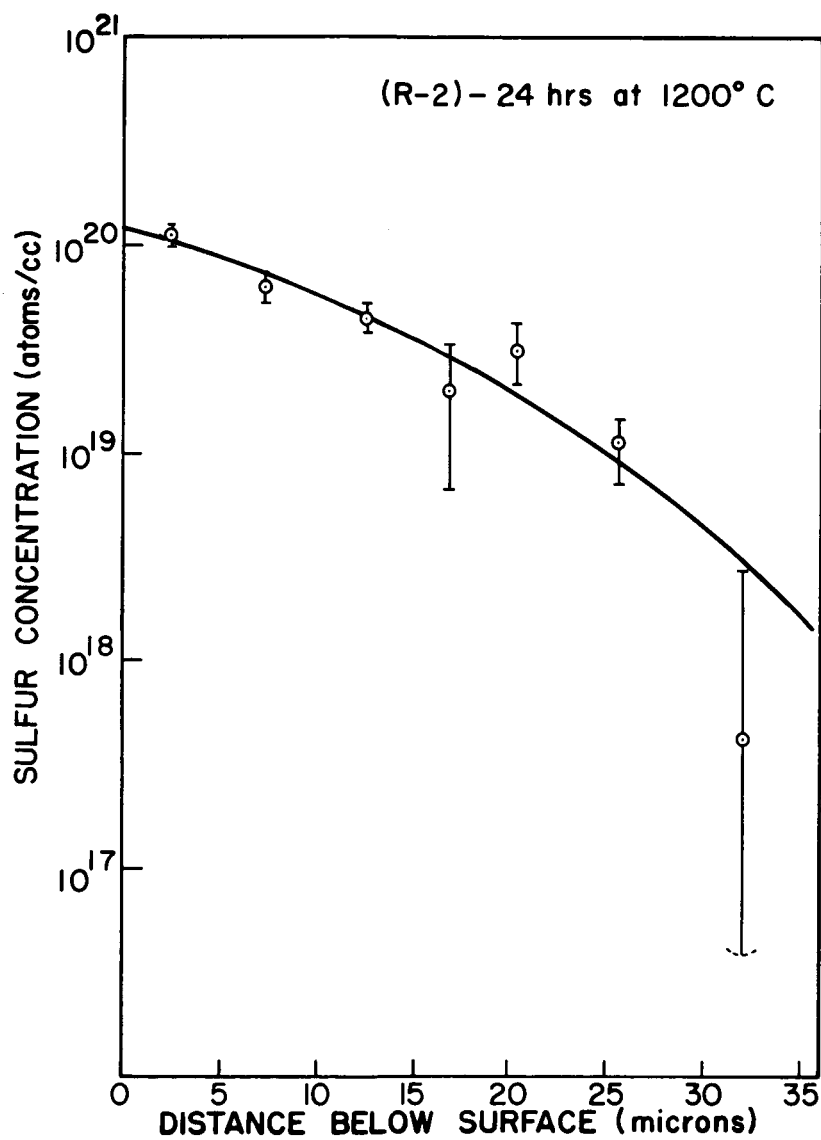


FIGURE 1

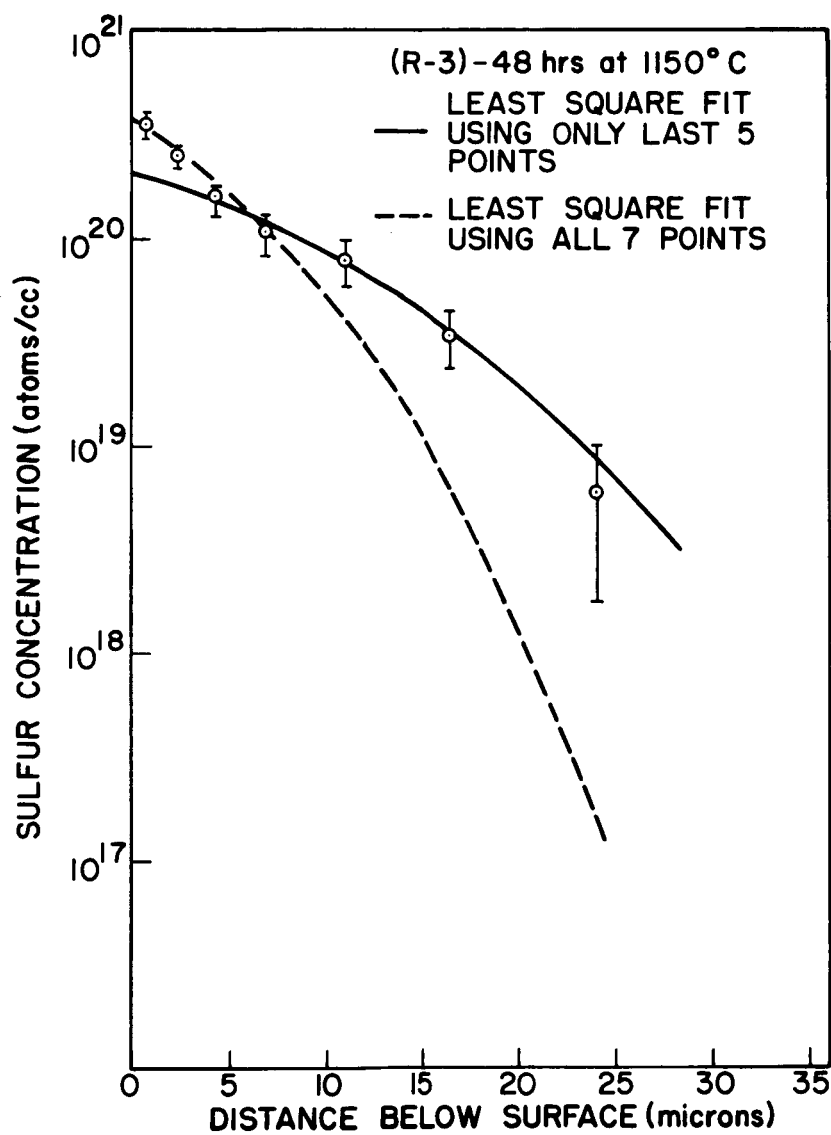


FIGURE 2